

# Interplay between superconductivity and magnetism in triangular lattices

Kun Woo Kim<sup>1,\*</sup> and T. Pereg-Barnea<sup>2</sup>

<sup>1</sup>*Department of Physics, Chung-Ang University, 06974 Seoul, Republic of Korea*

<sup>2</sup>*Department of Physics, McGill University, Montreal, Quebec, Canada H3A 2T8*

 (Received 22 July 2023; revised 17 October 2023; accepted 25 October 2023; published 8 November 2023)

Inspired by recent advances in the fabrication of surface superlattices, and in particular the triangular lattice made of tin (Sn) atoms on silicon, we study an extended Hubbard model on a triangular lattice. The observations of magnetism in these systems justify the inclusion of a strong on-site repulsion, and the observation of superconductivity suggests including an effective, nearest-neighbor attractive interaction. The attractive interaction mimics the effect of strong on-site repulsion near half filling, which can be seen in strong-coupling vertex calculations such as the Eliashberg method. With this extended Hubbard model on a triangular lattice with its geometrical frustration, we find a rich phase diagram of various magnetic orders and pairing functions, within the framework of self-consistent mean field theory. We uncover the competition between magnetism and unconventional superconductivity, and their coexistence for triplet pairings. We follow the Fermi surface of the system as the system is doped away from half filling and find nesting vectors and a Lifshitz transition, which provide an intuitive understanding of the phase transitions between the many orders we consider.

DOI: [10.1103/PhysRevB.108.195113](https://doi.org/10.1103/PhysRevB.108.195113)

## I. INTRODUCTION

Recent theoretical studies of superconductivity in triangular lattice systems have been motivated by a series of experimental investigations [1–4] where Sn adatoms placed on the surface of Si(111) form a two-dimensional triangular lattice, showing some evidence for unconventional chiral  $d$ -wave superconductivity. The magnetic ordering of the same superlattice system has been intensively studied as well, both theoretically and experimentally [5–8]. These kinds of systems combine the geometric frustration of the triangular lattice with strong electronic correlations and can, at least in theory, bring about a variety of states of matter such as a spin liquid, a collinear antiferromagnet, and spiral magnetic order at half filling as well as several unconventional superconducting orders away from half filling. Here, we explore the competition between magnetism and superconductivity in a wide range of doping and interaction strengths.

The studies of magnetic order in a triangular lattice described in Refs. [9–12] and other works investigate the possibility of unconventional superconductivity [13–17] and point to the possibility of both singlet and triplet superconductors with and without topological numbers. In this paper we focus on the competition between many order parameters, both magnetic and superconducting. We do so within the self-consistent mean field theory, where the on-site Hubbard  $U$  interaction favors magnetic order while pairing on bonds is favored by an attraction term on nearest-neighbor sites. This attraction is an effective description of strong correlations; the result of a Coulomb repulsion and Fermi surface nesting [14]. The tight-binding model in the triangular model comes with long-range hopping, sharpening the saddle of the dispersion

relation. We not only confirm the appearance of chiral  $d$ -wave superconductivity and collinear antiferromagnetic ordering as reported in experiments, but also find triplet pairing and spiral magnetic ordering at other fillings and interaction strengths. Crucially, we provide direct and intuitive understanding of magnetic phases from Fermi surface nesting and can relate the favored superconducting state to a synergy between the Fermi surface and the pairing function such that nodes are avoided and gaps are maximized.

The organization of this paper is the following. In Sec. II we introduce a model with on-site repulsion and nearest-neighbor attraction, and then the mean field Hamiltonian with magnetism and superconductivity is constructed. In Sec. III we construct the grand potential and derive the self-consistency relations for multiple order parameters. In Secs. IV and V we present our results and discuss them.

## II. EXTENDED HUBBARD MODEL ON A TRIANGULAR LATTICE

The kinetic part of our Hamiltonian is composed of tight-binding hopping parameters  $t_l$  between the  $l$ th neighbors on the triangular lattice, proposed to match angle-resolved photoemission spectroscopy (ARPES) data in Ref. [8]. The parameters were chosen to fit the lowest energy band of the Sn/Si(111) surface:

$$\hat{H}_0 = \sum_{l=1}^6 t_l \sum_{\langle ij \rangle_l} \hat{c}_i^\dagger \hat{c}_j, \quad (1)$$

where  $t_1 = -52.7$  meV and the longer-range hopping amplitudes  $t_2/t_1, \dots, t_6/t_1$  are  $-0.3881, 0.1444, -0.0228, 0,$  and  $-0.0318$ , respectively. The indices  $\langle i, j \rangle_l$  run over all pairs of  $l$ th-nearest-neighbor sites. The Fermi surface is depicted as a function of filling in Fig. 1(b) along with the density of

\*Corresponding author: [kunx@cau.ac.kr](mailto:kunx@cau.ac.kr)

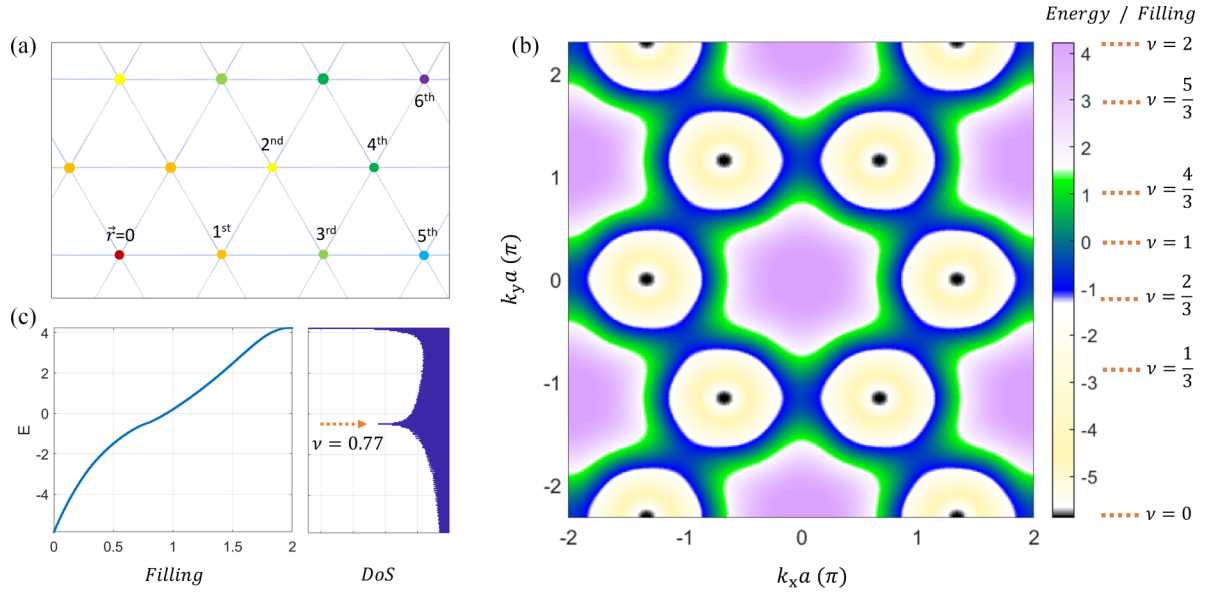


FIG. 1. (a) A triangular lattice with six nearest neighbors of the central atom (in red) marked with different colors. (b) The dispersion relation  $E(k_x, k_y)$  and the filling  $\nu = \langle \hat{n}_{i\uparrow} + \hat{n}_{i\downarrow} \rangle \equiv \langle \hat{n}_i \rangle$ . Energy is given in units of the nearest-neighbor hopping amplitude,  $|t_1| = 52.8$  meV. (c) The relation between filling and energy and between the DoS and energy.

states (DoS) as a function of energy. We include the on-site and extended Hubbard interaction terms:

$$\hat{H}_{\text{int}} = \sum_i U_0 \hat{n}_{i\uparrow} \hat{n}_{i\downarrow} + \sum_{(ij), \sigma\sigma'} U_1 \hat{n}_{i\sigma} \hat{n}_{j\sigma'}, \quad (2)$$

where we take  $U_0 > 0$  (repulsive) and  $U_1 < 0$  (attractive) as an effective description resulting from the spin fluctuation. With regard to the attractive density-density interaction, Cooper pairing indeed will never arise from repulsive interaction in the mean field approach. However, strong repulsive interactions do lead to superconductivity, especially in the vicinity of magnetic orders. This has been demonstrated in models for the cuprates (see, for example, Refs. [18–20]). Calculating the pairing vertex could be done in the Eliashberg formalism but, unfortunately, an effective attraction only emerges as an intermediate step. However, this approach may quickly become prohibitively complicated if one would like to consider magnetic orders as well. We therefore chose a different path: including both repulsive and attractive interactions and treating them both in the mean field. The on-site repulsive interaction favors magnetism. It is convenient to express the Hubbard  $U_0$  term as (Appendix A)

$$\hat{H}^{(\text{on})} = \sum_i U_0 \left[ \frac{1}{4} \hat{n}_i \hat{n}_i - \hat{S}_{im} \hat{S}_{im} \right], \quad (3)$$

where  $\hat{n}_i = \hat{n}_{i\uparrow} + \hat{n}_{i\downarrow}$  is the occupancy at site  $i$ , with  $\langle \hat{n}_i \rangle \in [0, 2]$ . The spin operator at site  $i$  in direction  $\hat{m}$  is defined as  $\hat{S}_{im} = \frac{1}{2} \sum_{\sigma\sigma'} \hat{c}_{i\sigma}^\dagger (\vec{\sigma} \cdot \hat{m})_{\sigma\sigma'} \hat{c}_{i\sigma'}$ , where  $\vec{\sigma}$  is the vector of Pauli matrices. We can therefore define a local spin order parameter as  $\vec{m} = \langle \hat{S}_{im} \rangle$ , where the direction of  $\vec{m}$  may give either ferromagnetic (FM) order or antiferromagnetic (AFM) order with collinear or spiral spin directions as depicted in Fig. 2(b). The magnitude  $m = |\vec{m}|$  represents the strength of

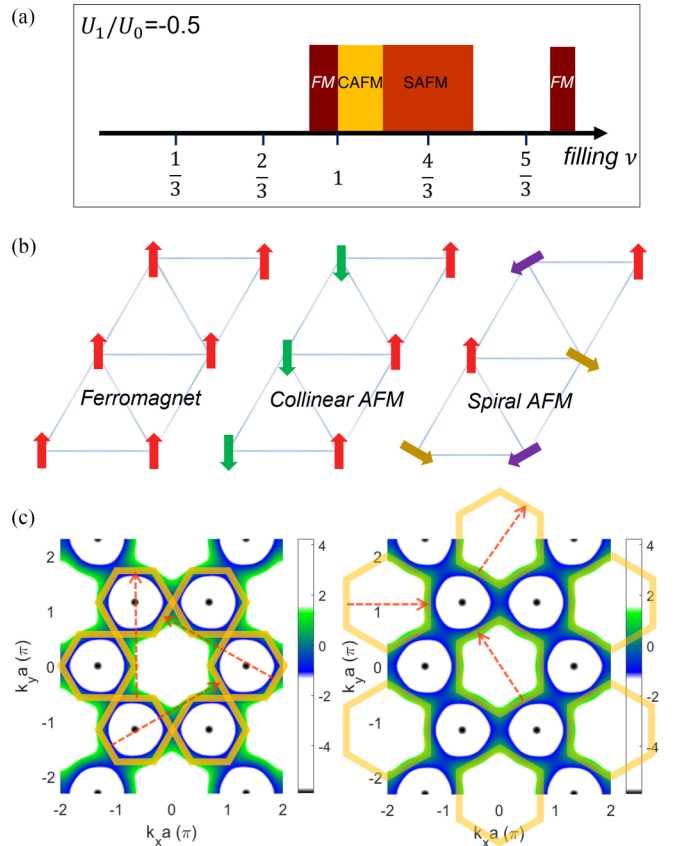


FIG. 2. (a) The phase diagram at  $U_1/U_0 = -0.5$ . (b) Three types of magnetic orderings. (c) The collinear AFM and spiral AFM appear from the Fermi surface nesting depicted. The ferromagnetism appears from the Stoner's criterion.

the order. The mean field Hamiltonian is then given by

$$\hat{H}_{\text{MF}}^{(\text{on})} = -U_0 N_{\text{lat}} \left[ \frac{1}{4} \langle \hat{n}_i \rangle^2 - |\bar{m}|^2 \right] + U_0 \sum_i \left[ \hat{c}_{i\uparrow}^\dagger \hat{c}_{i\downarrow}^\dagger \right] \left[ \frac{1}{2} \langle \hat{n}_i \rangle \sigma_0 - \bar{m} \cdot \vec{\sigma} \right] \begin{pmatrix} \hat{c}_{i\uparrow} \\ \hat{c}_{i\downarrow} \end{pmatrix}, \quad (4)$$

where the first term describes the on-site potential energy cost of having the magnetic order while the second term provides a possible energy benefit from a spin splitting. Note that the band energy shifts by  $\frac{1}{2} \langle \hat{n}_i \rangle \sigma_0$  due to the mean repulsive energy from the on-site interaction. To take into account the collinear and spiral antiferromagnetism, we extended the unit cell to include two or three atoms with rotated spins in our calculations.

The attractive interaction  $U_1 < 0$  can induce superconductivity or a charge density wave. We focus on superconductivity using, BCS-like, the self-consistent mean field:

$$\hat{H}_{\text{MF}}^{(\text{nn})} = -U_1 \sum_{(ij), \sigma\sigma'} |\Delta_{ji, \sigma'\sigma}|^2 + U_1 \sum_{(ij), \sigma, \sigma'} [c_{i, \sigma}^\dagger c_{j, \sigma'}^\dagger \Delta_{ji, \sigma'\sigma} + \Delta_{ij, \sigma\sigma'}^* c_{j\sigma'} c_{i\sigma}]. \quad (5)$$

The superconducting order parameter  $\Delta_{ji, \sigma'\sigma} = \langle c_{j\sigma'} c_{i\sigma} \rangle$  may describe either singlet or triplet spin pairing with  $s$ -,  $p$ -,  $d$ -, or  $f$ -wave spatial symmetry. We consider superconductivity and magnetism together to determine which combination of order parameters yields the lowest grand potential. It is worth noting that in order to consider superconductivity and magnetism simultaneously, the Hamiltonian in Eq. (4) needs to be written in the Bogoliubov–de Gennes (BdG) form with particle-hole symmetry (PHS; see Appendix B). The mean field Hamiltonian is

$$\hat{H}_{\text{MF}} = E_0(n_i, \bar{m}, \tilde{\Delta}_{ji, \sigma'\sigma}^{(s/t)}) + \frac{1}{2} \sum_k \Psi^\dagger \begin{pmatrix} H_{kk} & & & \tilde{\Delta}_{k, -k} \\ & H_{-k, -k} & \tilde{\Delta}_{-k, k} & \\ & -\tilde{\Delta}_{k, -k}^* & -H_{kk}^* & \\ -\tilde{\Delta}_{-k, k}^* & & & -H_{-k, -k}^* \end{pmatrix} \Psi, \quad (6)$$

where  $\tilde{\Delta}_{k'k''} = U_1 \Delta_{k'k''}$  and  $H_{k'k''}$  are  $2 \times 2$  matrices in spin space and  $\frac{1}{2}\text{BZ}$  is half the Brillouin zone. The BdG Hamiltonian is written in the basis  $\Psi^\dagger = (c_{k\uparrow}^\dagger, c_{k\downarrow}^\dagger, c_{-k\uparrow}^\dagger, c_{-k\downarrow}^\dagger, c_{k\uparrow}, c_{k\downarrow}, c_{-k\uparrow}, c_{-k\downarrow})$ . The constant energy  $E_0(n_i, \bar{m}, \tilde{\Delta}_{ji, \sigma'\sigma}^{(s/t)})$  contains the usual BCS ground state energy as well as terms resulting from the anticommutation relation of the operators which compose the magnetic order parameters:

$$E_0 = -U_0 N_{\text{lat}} \left[ \frac{1}{4} \langle \hat{n}_i \rangle^2 - |\bar{m}|^2 \right] + \frac{1}{2} U_0 N_{\text{lat}} \langle \hat{n}_i \rangle - U_1 \sum_{(ij), \sigma\sigma'} |\Delta_{ji, \sigma'\sigma}|^2. \quad (7)$$

The Hamiltonian written in this structure visibly satisfies the particle-hole symmetry which is represented by the operator  $\mathcal{P} = K\tau_x$ , where  $K$  is complex conjugation and the

Pauli matrix  $\tau_x$  exchanges particles and holes, such that  $\mathcal{P}H_{\text{BdG}}\mathcal{P}^{-1} = -H_{\text{BdG}}$  (see Appendix B for a discussion of the PHS in the basis  $\Psi^\dagger$ ). The block-diagonal Hamiltonian in Eq. (6) is

$$H_{kk} = [\epsilon_{\vec{k}} + \frac{1}{2} U_0 \langle \hat{n}_i \rangle] \sigma_0 - \bar{m} \cdot \vec{\sigma}, \quad (8)$$

where  $\epsilon_{\vec{k}}$  is the Fourier transform of Eq. (1) (see Ref. [21] for its explicit expression). The summation over crystal momentum is on half of the Brillouin zone because our basis contains both the  $|k\sigma\rangle$  and  $|-k\sigma\rangle$  states. The BdG Hamiltonian ( $8 \times 8$ ) in the full basis is block diagonal with two  $4 \times 4$  blocks with opposite signs of eigenvalues. Note that one could choose to either work with this  $8 \times 8$  block-diagonal Hamiltonian and sum over half of the Brillouin zone or work with only one of the blocks and sum over the entire Brillouin zone. The pairing potential  $\Delta_{k, -k}$  is given by

$$(\Delta_{k, -k})_{\sigma\sigma'} = \sum_{\vec{\delta}_{ji}} \Delta_{ji, \sigma'\sigma} e^{-i\vec{k} \cdot \vec{\delta}_{ji}},$$

where the sum is over the six nearest-neighbor vectors,  $\vec{\delta}_{ji} = \vec{r}_j - \vec{r}_i \in \{(1, 0), (\frac{1}{2}, \frac{\sqrt{3}}{2}), (-\frac{1}{2}, \frac{\sqrt{3}}{2}), (-1, 0), (-\frac{1}{2}, -\frac{\sqrt{3}}{2}), (\frac{1}{2}, -\frac{\sqrt{3}}{2})\}$ , with angles  $\theta_{ji} \in \{0, \frac{\pi}{3}, \frac{2\pi}{3}, \pi, \frac{4\pi}{3}, \frac{5\pi}{3}\}$  relative to the  $x$  axis. The symmetry of the pairing function in real space (odd or even with respect to exchanging the sites  $i$  and  $j$ ) determines whether the spins of the Cooper pair are in the singlet or triplet configuration such that  $\Delta_{ji, \sigma\sigma'}$  is antisymmetric to the exchange of both position and spin.

$$\Delta_{ji, \sigma\sigma'} = \chi_{\sigma\sigma'}^{(s/t)} \otimes \phi_{ji}^{(\text{even/odd})} \quad (9)$$

and

$$\chi^{(s)} = \begin{pmatrix} 0 & +\Delta_s \\ -\Delta_s & 0 \end{pmatrix}, \quad \chi^{(t)} = \begin{pmatrix} \Delta_{\uparrow\uparrow} & \Delta_t \\ \Delta_t & \Delta_{\downarrow\downarrow} \end{pmatrix}. \quad (10)$$

We label the spatial pairing functions by their angular momentum; the phase winding number around a central atom is such that for  $s$ -wave symmetry,  $\phi_{ji}^{(s)} = 1$ , and for angular momentum  $l$  a chiral pairing function winds  $l$  times and is given by  $\phi_{ji}^{(l)} \propto e^{il\theta_{jj'}}$ . However, since we do not want to impose chirality *a priori*, we minimize the mean field energy with two pairing functions for each angular momentum,

$$\phi_{ji}^{(p_x)} = \cos \theta_{ji}, \quad \phi_{ji}^{(p_y)} = \sin \theta_{ji}, \quad (11)$$

$$\phi_{ji}^{(d_{x^2-y^2})} = \cos 2\theta_{ji}, \quad \phi_{ji}^{(d_{xy})} = \sin 2\theta_{ji}, \quad (12)$$

$$\phi_{ji}^{(f_{x(x^2-3y^2)})} = \cos 3\theta_{ji}, \quad \phi_{ji}^{(f_{y(3x^2-y^2)})} = \sin 3\theta_{ji}, \quad (13)$$

such that the chiral  $p$ -,  $d$ -, or  $f$ -wave superconductivity is obtained if both pairing functions are non-zero and there is a  $\pi/2$  phase difference between them. Otherwise we end up with a nonchiral state. In the case of  $f$ -wave symmetry, the  $f_{y(3x^2-y^2)}$  is zero for nearest-neighbor links in the triangular lattice, and we therefore end up with a nonchiral, real order parameter of the form  $f_{x(x^2-3y^2)}$ . A chiral  $f$ -wave order would require longer-range attraction.

### III. SELF-CONSISTENCY EQUATIONS FOR ORDER PARAMETERS

The grand potential is obtained from the grand canonical partition function  $Z = \text{Tr} e^{-\beta(\hat{H}_{\text{MF}} - \mu\hat{N})}$  in the diagonal basis.

$$\hat{H}_{\text{MF}} - \mu\hat{N} = E_0 + \frac{1}{2} \sum_{k,\alpha}^{\frac{1}{2}\text{BZ}} [\zeta_{k,\alpha} \hat{\gamma}_{k\alpha}^\dagger \hat{\gamma}_{k\alpha} - \zeta_{k,\alpha} \hat{\gamma}_{k\alpha} \hat{\gamma}_{k\alpha}^\dagger], \quad (14)$$

where  $\alpha$  labels the eigenvalues and  $\zeta_{k,\alpha}$  is an eigenvalue of one sub-block BdG Hamiltonian (6). Due to particle-hole symmetry, the eigenvalues in the two sub-blocks of the Hamiltonian each have a pair of identical eigenvalues with opposite sign. Summing over all (single particle) eigenstates, we obtain the grand potential:

$$\Omega = -\frac{1}{\beta} \ln Z = E_0 - \frac{1}{\beta} \sum_{k,\alpha}^{\frac{1}{2}\text{BZ}} \ln \left[ 2 \cosh \frac{\beta \zeta_{k,\alpha}}{2} \right], \quad (15)$$

where the temperature  $\beta = k_B T = 0.1|t_1|$  is taken and the sum is only over positive  $\zeta_{k,\alpha}$  values [22]. The minimum of the grand potential is the self-consistent solution for the order parameters, and we therefore set the grand potential derivatives with respect to the order parameters to zero. We write the derivatives as (see Appendix C)

$$\frac{\partial \Omega}{\partial m_j} = \frac{\partial E_0}{\partial m_j} + \frac{\partial}{\partial m_j} [\Omega - E_0] = 0, \quad (16)$$

$$\frac{\partial \Omega}{\partial \Delta_\nu^*} = \frac{\partial E_0}{\partial \Delta_\nu^*} + \frac{\partial}{\partial \Delta_\nu^*} [\Omega - E_0] = 0, \quad (17)$$

where  $j \in \{x, y, z\}$  and  $\nu \in \{s, t, \uparrow\uparrow, \downarrow\downarrow\}$ . We solve the above conditions through iterations and update all order parameters at every step. Using the fact that the energy  $E_0$  contains  $\sum_{j=x,y,z} m_j^2$  and  $\Delta_\nu \Delta_\nu^*$ , we can update an order parameter through iteration. That is,

$$m_j^{(\text{new})} = m_j^{(\text{old})} \left[ 1 - \eta \frac{\partial \Omega}{\partial m_j} \left( \frac{\partial E_0}{\partial m_j} \right)^{-1} \right]_{\text{old}}, \quad (18)$$

$$\Delta_\nu^{(\text{new})} = \Delta_\nu^{(\text{old})} \left[ 1 - \eta \frac{\partial \Omega}{\partial \Delta_\nu^*} \left( \frac{\partial E_0}{\partial \Delta_\nu^*} \right)^{-1} \right]_{\text{old}}, \quad (19)$$

where the right-hand side is computed using a set of order parameters to be updated.  $\eta$  ( $\simeq 0.2$ ) controls the rate of approaching speed toward a convergence over iterations. When converged,  $m_j^{(\text{new})} = m_j^{(\text{old})}$  and  $\partial_{m_j} \Omega|_{\text{old}} = 0$ . The partial differentiation is numerically obtained by computing the difference of grand potentials,  $\partial_{m_j} \Omega \simeq \lim_{\Delta m_j \rightarrow 0} \Delta \Omega / \Delta m_j$ . The mean field Hamiltonian is also a function of filling  $\nu$ ; see Eq. (4). Along with other order parameters, the filling is updated in each iteration by computing

$$\nu = -\frac{1}{N_{\text{lat}}} \frac{\partial \Omega}{\partial \mu} = \langle \hat{n}_{i\uparrow} + \hat{n}_{i\downarrow} \rangle. \quad (20)$$

### IV. RESULTS: TOPOLOGICAL SUPERCONDUCTIVITY AND MAGNETISM

*Magnetic orders.* The Stoner criterion gives a heuristic rule for when magnetic order might develop; if the density of states at the Fermi level exceeds a critical value set by the

on-site repulsive interaction, magnetic order could develop to reduce the interaction energy. This intuition is indeed in line with our findings: Fig. 1(c) shows that at filling near  $\nu = 0.77$ , the DoS is peaked and this is where we find ferromagnetism. Another important factor in determining whether or not magnetism will appear and the kind of magnetism that will develop is the shape of the Fermi surface. A magnetic order which reduces the periodicity is most effective if its ordering vector connects many states near the Fermi level, i.e., opens a gap through nesting.

Around,  $\nu \sim 1$ , collinear antiferromagnetism appears. This order reduces the periodicity by folding the Brillouin zone in one of three directions; one such spin configuration is shown in Fig. 2(b). The periodicity of the collinear antiferromagnet (CAF) in real space is  $\sqrt{3}a$ , which doubles the size of the unit cell. Thus the size of the nesting vector  $|\vec{Q}_{\text{CAF}}| = 2\pi/\sqrt{3}a$  in momentum space is half of the shortest reciprocal lattice vector. The possible nesting Fermi surface lines are indicated in Fig. 2(c). However, since the CAFM ordering appears only in one direction, the Fermi surface is not fully gapped by this order, and the system remains metallic.

Right next to the CAFM order, the spiral antiferromagnetic (SAFM) is the most energetically favorable phase. The filling is a bit higher, and the corresponding Fermi surface is marked in green in Fig. 2(c). The size of the nesting vector is  $\frac{4\pi}{3a}$ , which is smaller than that in the CAFM case, while the directions of the three vectors are rotated by  $\pi/2$ . The spiral AFM gaps the Fermi surface completely, lowering the grand potential even more than the CAFM.

The development of the three magnetic orderings in a small doping range can be understood from the density of states (DoS) and the shape of the Fermi surface of the long-range-hopping tight-binding model in the triangular lattice model for filling  $\nu \in [0.8, 1.5]$ . The result of the self-consistent mean field with multiple order parameters is shown in Fig. 2(a) for  $U_0/|t_1| = 6$  and  $U_1/|t_1| = -3$ . The bandwidth of the hopping model in Eq. (1) ( $\sim 10|t_1|$ ) as shown in Fig. 1 is larger than the employed interaction strength. We note that previous authors [8] found that the CAFM is preferred over the SAFM at half filling  $\nu = 1$  using a more sophisticated numerical method. When the effective nearest-neighbor attraction  $U_1$  increases further, topological superconductivity appears next to the antiferromagnetic orders.

*Superconductivity.* The study of superconductivity (SC) in one-band triangular lattice models was ignited by the experimental observation of superconductivity in Sn/Si(111) [1,2]. We therefore set out to find out what kind of superconductivity can emerge from our effective nearest-neighbor attraction while on-site repulsion is present. This approach to interaction-based unconventional superconductivity provides an intuitive understanding of how order parameters compete to balance decreasing the interaction energy while increasing the kinetic energy through orderings. We therefore minimize our grand potential by considering both magnetism and superconductivity together. Figure 3(a) shows the phase diagram as a function of filling with  $U_1/U_0 = -0.8$ . The  $f$ -wave SC appears first, and as can be seen in Fig. 3(b), it has three pairs of line nodes. For filling  $\nu \in [0.2, 0.7]$ , the Fermi surface is located where the nodal lines are avoided, and therefore the

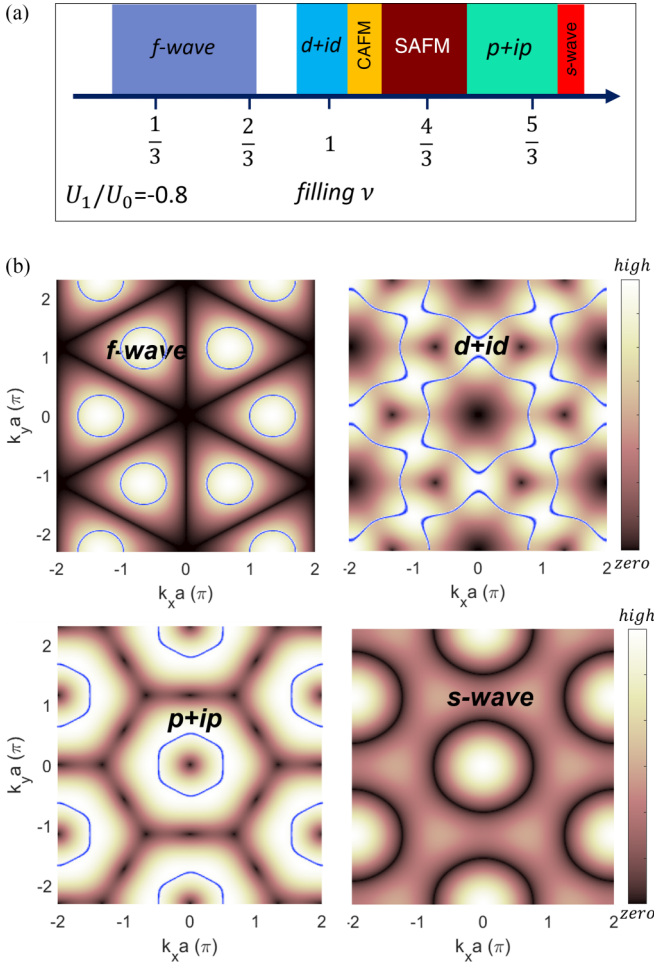


FIG. 3. (a) The phase diagram at  $U_1/U_0 = -0.8$ . Chiral  $d$ -wave and  $p$ -wave superconductivity appears next to the antiferromagnetic orderings. At lower and higher filling,  $f$ -wave and  $s$ -wave superconductivity appears, respectively. (b) The magnitude of pairing  $|\Delta_{\mathbf{k}, -\mathbf{k}\sigma\sigma'}^{(\text{pairing})}|$  is plotted for the orbital symmetries. The overlaid Fermi surface (blue lines) at fillings  $\nu = 1/3, 1, 5/3$  shows that nodal lines of the pairing are avoided, maximizing the superconducting energy gap opening.

$f$ -wave pairing fully gaps the system, reducing the interaction energy which results from  $U_1$ .

As the filling is increased beyond 0.7, the Fermi surface undergoes a Lifshitz transition from six pockets to a single snowflake-shaped surface at the center of the Brillouin zone. Once the transition has occurred, the  $f$ -wave symmetry cannot fully gap the Fermi surface, and the preferred pairing changes. The Fermi surface that favors the CAFM order for reducing the on-site interaction energy favors the chiral  $d + id$  superconductor for reducing the  $U_1$  interaction energy. The competition between the two phases is studied by minimizing the grand potential with the two orders present, and this yields the result that a  $d + id$  superconductor appears before the collinear antiferromagnet.

Around  $\nu = 3/4$  the spiral antiferromagnet is favored (despite the significant  $U_1$ ), but at higher filling of  $\nu > 1.5$  another topological superconductor with  $p + ip$  structure is developed. This order parameter has nodal points which are

avoided by the small Fermi surface around the zone center as shown in the bottom left panel of Fig. 3(b) such that the Fermi surface is fully gapped.

Lastly, when every site is nearly fully filled,  $\nu \sim 2$ , the  $s$ -wave pairing potential which has a circular line node away from  $\vec{k} = 0$  is preferred. At high filling, there is a transition from the ferromagnetic ordering to the  $s$ -wave superconductivity with increasing attractive extended interaction strength  $|U_1|$ ; see Fig. 4(a).

We note that the order of superconducting phases (chiral  $p$ -wave and  $f$ -wave symmetries) we find is inconsistent with that of Wolf *et al.* [14,16] but it is consistent with that of Cheng *et al.* [13]. While we rely on an effective interaction for our mean field calculations, we believe that the filling in which we find the various orders is very plausible since it is compatible with the intuition provided by the Fermi surface shapes at the various fillings as discussed above.

*From magnetic ordering to superconducting.* The phase diagram is drawn in Fig. 4(a) for  $U_1/U_0 \in [-0.2, 1.2]$ . At small  $U_1$  only magnetic orders appear. For  $U_1/U_0 < -0.4$ , superconductivity begins to appear. While the singlet pairing does not coexist with the magnetic orderings, the triplet pairing may. We verify the coexistence and also plot the superconductor and the magnetic order parameters separately in Figs. 4(b) and 4(c), respectively. In particular,  $f$ -wave superconductivity coexists with ferromagnetism near  $\nu = 0.75$ , and the CAFM and SAFM orders give way to  $p + ip$  pairing when  $|U_1|$  is increased.

## V. CONCLUSIONS

In this paper we explored the possibility of magnetic and superconducting orders in the extended Hubbard model on a triangular lattice. Our model includes a repulsive on-site Hubbard interaction  $U_0$  and an effective nearest-neighbor attractive interaction  $U_1$ . We treat the model with the variational, self-consistent mean field theory, which considers a large set of magnetic and superconducting orders together. We map the phase diagram and find a ferromagnetic phase and two antiferromagnetic phases when the attractive interaction is weak. For higher values of the attractive interaction we find superconducting states with  $s$ -,  $d$ -,  $p$ -, and  $f$ -wave symmetry. The  $p$ -wave and  $d$ -wave superconducting order parameters are found to be chiral or topological.

Near filling  $\nu = 1-1.5$  the collinear antiferromagnetism and the spiral magnetism are consistent with previous studies [8] and are found to coexist with a  $p + ip$  triplet topological superconductivity when the attractive interaction is significant. Our finding of  $f$ -wave and  $(p + ip)$ -wave superconductivity at low and high filling is also consistent with a previous study [13], and we find a  $d + id$  topological superconductor to emerge when long-range hopping is included in the kinetic energy. The recent observation of the chiral superconductivity in Sn/Si(111) at half filling [4], the experimental relevance of our study, and Fig. 4 indicate that other unconventional superconductivity and magnetic orderings are nearby in the phase diagram.

Our study has been inspired by recent advances in surface manipulation and, in particular, the creation of a triangular superlattice of tin atoms on a silicon surface [9–12]. However,

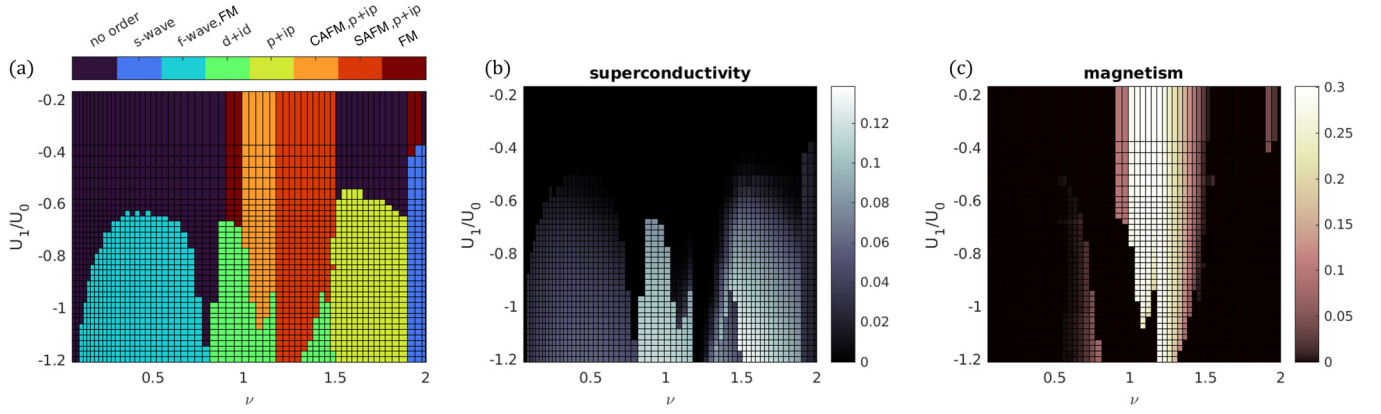


FIG. 4. (a) The phase diagram as a function of filling  $\nu$  and the attractive interaction strength  $U_1$  for  $U_0 = 6|t_1|$ . (b) and (c) The corresponding superconducting  $|\Delta_\alpha|$  and magnetic order parameters  $|m_\alpha|$  are plotted in the same domain. They show the portion of order parameters for magnetism coexisting with triplet-pairing superconductivity:  $(p + ip)$ -wave and  $f$ -wave SC. See Figs. 5 and 6 for complete information about the grand potential, the order parameters, and their temperature dependence at  $U_1/U_0 = -0.8$ .

we expect these results to hold for other similar compounds. In particular, our finding of chiral topological superconductivity could lead to the realization of Majorana zero modes at vortex cores in these compounds. The proximity of these phases to other, nontopological phases suggests that the existence of Majorana modes could be controlled through gating and external fields.

Lastly, we would like to add a note about temperature. Due to our limited momentum resolution we could not perform calculations at a very low temperature and used  $\beta = k_B T = 0.1|t_1| = 5.28$  meV, which corresponds to  $\sim 61$  K. This meant that in order to see gaps open, we needed to work with large interaction values. We therefore believe that at lower temperature, one could see superconductivity with even weaker interactions.

### ACKNOWLEDGMENTS

K.W.K. acknowledges that this research was supported by Chung-Ang University research grants in 2021. T.P.-B. acknowledges support from the Natural Sciences and Engineering Research Council of Canada (NSERC).

### APPENDIX A: MEAN FIELD DECOMPOSITION OF THE HUBBARD INTERACTION

The on-site Hubbard interaction can be written as the density and spin operators using  $\hat{n}_{i\uparrow} = \sum_{\alpha\beta} \frac{1}{2}(1 + \sigma_z)_{\alpha\beta} \hat{c}_{i\alpha}^\dagger \hat{c}_{i\beta}$ . More generally, the interaction can be written on the basis of arbitrary spin direction  $\sigma_l = \hat{l} \cdot \vec{\sigma}$ . Dropping the site index,

$$\begin{aligned} \hat{n}_\uparrow \hat{n}_\downarrow &= \sum_{\alpha\beta\gamma\delta} \frac{1}{4} (1 + \sigma_l)_{\alpha\beta} (1 - \sigma_l)_{\gamma\delta} \hat{c}_{i\alpha}^\dagger \hat{c}_{i\beta} \hat{c}_{i\gamma}^\dagger \hat{c}_{i\delta} \\ &= \sum_{\alpha\beta\gamma\delta} \frac{1}{4} (\delta_{\alpha\beta} \delta_{\gamma\delta} - (\sigma_l)_{\alpha\beta} (\sigma_l)_{\gamma\delta}) \hat{c}_{i\alpha}^\dagger \hat{c}_{i\beta} \hat{c}_{i\gamma}^\dagger \hat{c}_{i\delta}, \end{aligned}$$

where from the first line to the second the following relation is used:  $\sum_{\alpha\beta\gamma\delta} (\sigma_l)_{\gamma\delta} \delta_{\alpha\beta} \hat{c}_{i\alpha}^\dagger \hat{c}_{i\beta} \hat{c}_{i\gamma}^\dagger \hat{c}_{i\delta} = \sum_{\alpha\beta\gamma\delta} (\sigma_l)_{\alpha\beta} \delta_{\gamma\delta} \hat{c}_{i\alpha}^\dagger \hat{c}_{i\beta} \hat{c}_{i\gamma}^\dagger \hat{c}_{i\delta}$ .

As a result,

$$\hat{H}^{(\text{on})} = U_0 \sum_i \left[ \frac{1}{4} \hat{n}_i \hat{n}_i - \hat{S}_{il} \hat{S}_{il} \right], \quad (\text{A1})$$

where  $\hat{n}_{i\sigma} = \hat{c}_{i\sigma}^\dagger \hat{c}_{i\sigma}$  and  $\hat{S}_{il} = \frac{1}{2} \sum_{\alpha,\beta} \hat{c}_{i\alpha}^\dagger (\hat{l} \cdot \vec{\sigma})_{\alpha\beta} \hat{c}_{i\beta}$ . Neglecting the fluctuating part of the interaction, the mean field approximation is

$$\hat{n}_i^2 \simeq 2\hat{n}_i \langle \hat{n}_i \rangle - \langle \hat{n}_i \rangle^2, \quad (\text{A2})$$

$$\hat{S}_{il}^2 \simeq 2\hat{S}_{il} \langle \hat{S}_{il} \rangle - \langle \hat{S}_{il} \rangle^2. \quad (\text{A3})$$

The mean field Hamiltonian (4) is obtained.

### APPENDIX B: PARTICLE-HOLE SYMMETRY AND GRAND POTENTIAL

The BdG Hamiltonian (6) can be written as the sum of two sub-blocks:

$$\begin{aligned} \hat{H} - \mu \hat{N} &= \frac{1}{2} \sum_k^{\frac{1}{2}\text{BZ}} \begin{pmatrix} \hat{C}_k^\dagger & \hat{C}_{-k} \end{pmatrix} \begin{pmatrix} \tilde{H}_{k,k} & \tilde{\Delta}_{k,-k} \\ -\tilde{\Delta}_{-k,k}^* & -\tilde{H}_{-k,-k} \end{pmatrix} \begin{pmatrix} \hat{C}_k \\ \hat{C}_{-k}^\dagger \end{pmatrix} \\ &+ \frac{1}{2} \sum_k^{\frac{1}{2}\text{BZ}} \begin{pmatrix} \hat{C}_k & \hat{C}_{-k}^\dagger \end{pmatrix} \begin{pmatrix} -\tilde{H}_{k,k} & -\tilde{\Delta}_{k,-k} \\ \tilde{\Delta}_{-k,k}^* & \tilde{H}_{-k,-k} \end{pmatrix}^* \begin{pmatrix} \hat{C}_k \\ \hat{C}_{-k}^\dagger \end{pmatrix}, \end{aligned} \quad (\text{B1})$$

where  $\hat{C}_k^\dagger = (c_{k\uparrow}^\dagger \ c_{k\downarrow}^\dagger)$  and  $\tilde{H}_{k,k} = H_{k,k} - \mu$ . The Hermiticity of the sub-block Hamiltonians is guaranteed because  $\Delta^T = -\Delta$ . By the diagonalization,

$$\begin{pmatrix} \tilde{H}_{k,k} & \tilde{\Delta}_{k,-k} \\ -\tilde{\Delta}_{-k,k}^* & -\tilde{H}_{-k,-k} \end{pmatrix} = U \begin{pmatrix} \zeta_1 & 0 \\ 0 & \zeta_2 \end{pmatrix} U^\dagger, \quad (\text{B2})$$

$$\begin{pmatrix} -\tilde{H}_{k,k} & -\tilde{\Delta}_{k,-k} \\ \tilde{\Delta}_{-k,k}^* & \tilde{H}_{-k,-k} \end{pmatrix}^* = U^* \begin{pmatrix} -\zeta_1 & 0 \\ 0 & -\zeta_2 \end{pmatrix} U^T, \quad (\text{B3})$$

which verifies that the BdG Hamiltonian (6) contains pairs of eigenvalues with the same magnitude and the opposite sign. Note that in general,  $\zeta_1 \neq -\zeta_2$  when  $\tilde{H}_{k,k} \neq \tilde{H}_{-k,-k}$ . Thus,

within each sub-block Hamiltonian, there is no particle-hole symmetry as is sometimes assumed in the literature. The full spin and particle-hole basis must be employed for a system without inversion symmetry. In the eigenstate basis, the Hamiltonian can be written as

$$\begin{aligned} \hat{H} - \mu\hat{N} = & \frac{1}{2} \sum_k^{\frac{1}{2}\text{BZ}} (\hat{\gamma}_{k,1}^\dagger \quad \hat{\gamma}_{k,2}^\dagger) \begin{pmatrix} \zeta_{k,1} & 0 \\ 0 & \zeta_{k,2} \end{pmatrix} \begin{pmatrix} \hat{\gamma}_{k,1} \\ \hat{\gamma}_{k,2} \end{pmatrix} \\ & + \frac{1}{2} \sum_k^{\frac{1}{2}\text{BZ}} (\hat{\gamma}_{k,1} \quad \hat{\gamma}_{k,2}) \begin{pmatrix} -\zeta_{k,1} & 0 \\ 0 & -\zeta_{k,2} \end{pmatrix} \begin{pmatrix} \hat{\gamma}_{k,1}^\dagger \\ \hat{\gamma}_{k,2}^\dagger \end{pmatrix}, \end{aligned} \quad (\text{B4})$$

where  $(\hat{\gamma}_{k,1}^\dagger \quad \hat{\gamma}_{k,2}^\dagger) = (\hat{C}_k^\dagger \quad \hat{C}_{-k})U$  and  $U^* = U^{\dagger T}$  are used. This is the mean field Hamiltonian equation (14) used for the construction of the grand canonical partition function.

Let us deduce the PHS relation that the block Hamiltonian matrix satisfies. The second term in Eq. (B1) can be written as

$$\begin{aligned} \hat{H} - \mu\hat{N} = & \frac{1}{2} \sum_k^{\frac{1}{2}\text{BZ}} (\hat{C}_k^\dagger \quad \hat{C}_{-k}) \begin{pmatrix} \tilde{H}_{k,k} & \tilde{\Delta}_{k,-k} \\ -\tilde{\Delta}_{-k,k}^* & -\tilde{H}_{-k,-k}^* \end{pmatrix} \begin{pmatrix} \hat{C}_k \\ \hat{C}_{-k}^\dagger \end{pmatrix} \\ & + \frac{1}{2} \sum_k^{\frac{1}{2}\text{BZ}} (\hat{C}_{-k}^\dagger \quad \hat{C}_k) \tau_x \begin{pmatrix} -\tilde{H}_{k,k} & -\tilde{\Delta}_{k,-k} \\ \tilde{\Delta}_{-k,k}^* & \tilde{H}_{-k,-k}^* \end{pmatrix}^* \\ & \times \tau_x \begin{pmatrix} \hat{C}_{-k}^\dagger \\ \hat{C}_k \end{pmatrix}. \end{aligned} \quad (\text{B5})$$

The first term on the right-hand side is the sum over momentum in one-half of the Brillouin zone, and the second term is over the other half. The Hamiltonian in the second term is related to the first one by the following relation:

$$H_{\text{bld}}(-k) = \tau_x \begin{pmatrix} -\tilde{H}_{k,k} & -\tilde{\Delta}_{k,-k} \\ \tilde{\Delta}_{-k,k}^* & \tilde{H}_{-k,-k}^* \end{pmatrix}^* \tau_x \quad (\text{B6})$$

$$= -\tau_x \mathcal{K} H_{\text{bld}}(k) \tau_x \mathcal{K}, \quad (\text{B7})$$

where the subscript ‘‘bld’’ (for ‘‘block diagonal’’) indicates the Hamiltonian matrices in Eq. (B5).  $H_{\text{bld}}(k)$  is the Hamiltonian matrix in the first term on the right-hand side.

Next, let us deduce the PHS relation when the Hamiltonian matrix is constructed in the extended basis (also see the pedagogical note in Ref. [23]) as in Eq. (6). There is a unitary transformation between creation operators in real and momentum space:

$$\Psi_k = \begin{pmatrix} \vec{C}_k \\ \vec{C}_k^\dagger \end{pmatrix} = \begin{pmatrix} V & \\ & V^* \end{pmatrix} \begin{pmatrix} \vec{C}_r \\ \vec{C}_r^\dagger \end{pmatrix}, \quad (\text{B8})$$

where the Fourier transformation  $(V)_{ij} = \frac{1}{\sqrt{N_{\text{lat}}}} e^{-ik_i \cdot \vec{r}_j}$  and

$$\vec{C}_k = (c_{k_1}, \dots, c_{k_N})^T, \quad (\text{B9})$$

$$\vec{C}_k^\dagger = (c_{k_1}^\dagger, \dots, c_{k_N}^\dagger)^T, \quad (\text{B10})$$

$$\vec{C}_r = (c_{r_1}, \dots, c_{r_N})^T, \quad (\text{B11})$$

$$\vec{C}_r^\dagger = (c_{r_1}^\dagger, \dots, c_{r_N}^\dagger)^T, \quad (\text{B12})$$

where spin and sublattice degrees of freedom can be added in the operator vectors. Let  $\Psi_r = \begin{pmatrix} \vec{C}_r \\ \vec{C}_r^\dagger \end{pmatrix}$ . Likewise,

$$\Psi_k^\dagger = \Psi_r^\dagger \begin{pmatrix} V^\dagger & \\ & V^{*\dagger} \end{pmatrix}. \quad (\text{B13})$$

Note that  $\Psi_k^\dagger$  and  $\Psi_k$  take the same form as the one used in the mean field Hamiltonian, Eq. (6). The Hamiltonian operator is

$$\hat{H} = \Psi_k^\dagger H_k \Psi_k = \Psi_r^\dagger \begin{pmatrix} V^\dagger & \\ & V^{*\dagger} \end{pmatrix} H_k \begin{pmatrix} V & \\ & V^* \end{pmatrix} \Psi_r \quad (\text{B14})$$

$$= -\Psi_r^\dagger \tau_x \mathcal{K} \begin{pmatrix} V^\dagger & \\ & V^{*\dagger} \end{pmatrix} H_k \begin{pmatrix} V & \\ & V^* \end{pmatrix} \tau_x \mathcal{K} \Psi_r \quad (\text{B15})$$

$$= -\Psi_r^\dagger \begin{pmatrix} V^\dagger & \\ & V^{*\dagger} \end{pmatrix} \tau_x \mathcal{K} H_k \tau_x \mathcal{K} \begin{pmatrix} V & \\ & V^* \end{pmatrix} \Psi_r \quad (\text{B16})$$

$$= \Psi_k^\dagger \tau_x (-H_k^*) \tau_x \Psi_k, \quad (\text{B17})$$

where in the second line we used  $H_r = -\tau_x \mathcal{K} H_r \tau_x \mathcal{K}$ . In the third line,

$$\tau_x \mathcal{K} \begin{pmatrix} V & \\ & V^* \end{pmatrix} \tau_x \mathcal{K} = \begin{pmatrix} V & \\ & V^* \end{pmatrix} \quad (\text{B18})$$

is used. As shown in the last line, the PHS relation in the momentum space is  $H_k = -\tau_x \mathcal{K} H_k \tau_x \mathcal{K}$ . This verifies that when the Hamiltonian is written in the basis containing the creation and annihilation operators with the same set of indices as in  $\Psi_r$  and  $\Psi_k$ , the particle-hole symmetry relation is equally applied in the form of  $\mathcal{P} H_r \mathcal{P} = -H_r$  and  $\mathcal{P} H_k \mathcal{P} = -H_k$ . Note the sign difference in momentum compared with Eq. (B6), which applies to block-diagonal Hamiltonian matrices in  $H_k$ .

### APPENDIX C: SELF-CONSISTENCY RELATIONS

The mean field Hamiltonian includes order parameters whose values are determined self-consistently. We start with some initial value for each order parameter and update the values at every iteration step in the following way. With the ‘‘old’’ set of order parameter values we calculate the mean field energies, which are then used to calculate the grand potential. The ‘‘new’’ set of order parameter values are then calculated from the grand potential, and the process is continued until conversions, when the values do not change between iterations.

Calculating the order parameter from the grand potential can be demonstrated for ferromagnetic order in the  $z$  direction,  $m_z$ . Differentiating the grand potential by  $m_z$  gives

$$\frac{\partial \Omega}{\partial m_z} = \frac{\partial(\Omega - E_0)}{\partial m_z} + \frac{\partial E_0}{\partial m_z}, \quad (\text{C1})$$

where  $\partial_{m_z} E_0 = U_0 N_{\text{lat}} (2m_z)$  and

$$\begin{aligned} \frac{\partial(\Omega - E_0)}{\partial m_z} &= -\beta^{-1} \frac{1}{Z} \frac{\partial Z}{\partial m_z} \\ &= -\frac{U_0}{Z} \text{Tr} \left[ \left( \sum_i \hat{c}_{i\uparrow}^\dagger \hat{c}_{i\uparrow} - \hat{c}_{i\downarrow}^\dagger \hat{c}_{i\downarrow} \right) e^{-\beta(\hat{H} - \mu\hat{N})} \right] \\ &\equiv -U_0 \left\langle \sum_i \hat{c}_{i\uparrow}^\dagger \hat{c}_{i\uparrow} - \hat{c}_{i\downarrow}^\dagger \hat{c}_{i\downarrow} \right\rangle. \end{aligned} \quad (\text{C2})$$

Therefore, when the minimum of the grand potential is found,  $\partial_{m_z} \Omega = 0$ ,

$$m_z = \frac{1}{2} \langle \hat{c}_{i\uparrow}^\dagger \hat{c}_{i\uparrow} - \hat{c}_{i\downarrow}^\dagger \hat{c}_{i\downarrow} \rangle, \quad (\text{C3})$$

which is consistent with the way the  $\hat{S}_{iz}$  operator is defined in Eq. (3). For CAFM and SAFM, we prepare the order parameter in an enlarged unit cell. The relative spin angle within the unit cell is arranged in such a way that it realizes the desired spin ordering and the strength of the magnetism is the order parameter which is found self-consistently.

The self-consistent relation for the superconducting order parameter similarly follows. Let us begin from the real-space expression (5).

$$\frac{\partial(\Omega - E_0)}{\partial \Delta_{ji,\sigma'\sigma}} = \frac{U_1}{Z} \text{Tr}[(\hat{c}_{i\sigma}^\dagger \hat{c}_{j\sigma'}^\dagger) e^{-\beta(\hat{H} - \mu\hat{N})}] \quad (\text{C4})$$

$$= U_1 \langle \hat{c}_{i\sigma}^\dagger \hat{c}_{j\sigma'}^\dagger \rangle, \quad (\text{C5})$$

where we pick a specific site index  $i, j$  for the pairing order parameter; hence there is no summation. Since  $\partial_{\Delta_{ji,\sigma'\sigma}} E_0 = -U_1 \Delta_{ji,\sigma'\sigma}^*$ , we arrive at

$$\Delta_{ji,\sigma'\sigma}^* = \langle \hat{c}_{i\sigma}^\dagger \hat{c}_{j\sigma'}^\dagger \rangle. \quad (\text{C6})$$

Note the positions of indices,  $(\Delta^\dagger)_{ij,\sigma\sigma'} = \Delta_{ji,\sigma'\sigma}^*$ . For a general search of superconductivity with a certain pairing symmetry, we transform the Hamiltonian to momentum space using  $\hat{c}_{i\sigma}^\dagger = \frac{1}{\sqrt{N_{\text{lat}}}} \sum_k e^{ikr_i} \hat{c}_{k\sigma}^\dagger$ :

$$H_{\text{SC}} = U_1 \sum_{k,\sigma\sigma'\delta} \Delta_{\delta,\sigma'\sigma} \hat{c}_{k\sigma}^\dagger \hat{c}_{-k\sigma'}^\dagger e^{-ik\delta} + \text{H.c.}, \quad (\text{C7})$$

where  $\delta$  goes over the six nearest-neighbor vectors. The summation in momentum is then divided in half. This is to prepare the BdG Hamiltonian where the basis  $\Psi^{(\dagger)}$  includes both  $k$  and  $-k$ .

$$\begin{aligned} H_{\text{SC}} &= U_1 \sum_{k,\sigma\sigma'} \left( \sum_{\delta} \Delta_{\delta,\sigma'\sigma} e^{-ik\delta} \right) \hat{c}_{k\sigma}^\dagger \hat{c}_{-k\sigma'}^\dagger \\ &+ U_1 \sum_{k,\sigma\sigma'} \left( \sum_{\delta} \Delta_{\delta,\sigma'\sigma} e^{ik\delta} \right) \hat{c}_{-k\sigma}^\dagger \hat{c}_{k\sigma'}^\dagger + \text{H.c.}, \end{aligned} \quad (\text{C8})$$

where the parentheses in the first and the second terms are  $\Delta_{k-k,\sigma\sigma'}$  and  $\Delta_{-kk,\sigma\sigma'}$  in the BdG Hamiltonian equation (6). The order parameter  $\Delta_{\delta,\sigma'\sigma} = \chi_{\sigma'\sigma} \phi_\delta$ , where the spin configuration is in  $\chi_{\sigma,\sigma'}$  and the desired order parameter structure is  $\phi_\delta$ , which encodes a uniform order parameter whose magnitude and phase may depend on the bond direction. The

magnitude of the order parameter is included in  $\chi_{\sigma'\sigma}$ , and we therefore find it iteratively by performing the differentiation of the grand potential,

$$\begin{aligned} \frac{\partial(\Omega - E_0)}{\partial \chi_{\sigma'\sigma}} &= \frac{U_1}{Z} \text{Tr} \left[ \left( \sum_{k\delta} \phi_\delta e^{-ik\delta} \hat{c}_{k\sigma}^\dagger \hat{c}_{-k\sigma'}^\dagger \right) e^{-\beta(\hat{H} - \mu\hat{N})} \right] \\ &= U_1 \sum_{k\delta} \phi_\delta e^{-ik\delta} \langle \hat{c}_{k\sigma}^\dagger \hat{c}_{-k\sigma'}^\dagger \rangle \\ &= U_1 \sum_{k\delta} \phi_\delta e^{-ik\delta} \frac{1}{N_{\text{lat}}} \left\langle \sum_i e^{-ikr_i} \hat{c}_{i\sigma}^\dagger \sum_j e^{ikr_j} \hat{c}_{j\sigma'}^\dagger \right\rangle, \end{aligned} \quad (\text{C9})$$

where in the last line we bring it back to real-space expression using  $\hat{c}_{k\sigma}^\dagger = \frac{1}{\sqrt{N_{\text{lat}}}} \sum_i e^{-ikr_i} \hat{c}_{i\sigma}^\dagger$ . The summation over momentum yields the delta function  $\delta(r_j - r_i - \delta)$ . As a result,

$$\begin{aligned} \frac{\partial(\Omega - E_0)}{\partial \chi_{\sigma'\sigma}} &= U_1 \sum_{r_i\delta} \phi_\delta \langle \hat{c}_{i\sigma}^\dagger \hat{c}_{i+\delta\sigma'}^\dagger \rangle \\ &= U_1 N_{\text{lat}} \sum_{\delta} \phi_\delta \langle \hat{\Delta}_{\delta,\sigma\sigma'}^\dagger \rangle \\ &= U_1 N_{\text{lat}} \langle \hat{\chi}_{\sigma\sigma'}^\dagger \rangle \sum_{\delta} |\phi_\delta|^2, \end{aligned} \quad (\text{C10})$$

where the summation over momentum is restored to the whole BZ by combining  $k$  and  $-k$  terms. The constant energy term provides

$$\begin{aligned} \partial_{\chi_{\sigma'\sigma}} E_0 &= -U_1 \sum_{ij} \partial_{\chi_{\sigma'\sigma}} |\Delta_{\delta,\sigma'\sigma}|^2 \\ &= -U_1 \chi_{\sigma'\sigma}^* N_{\text{lat}} \sum_{\delta} |\phi_\delta|^2, \end{aligned} \quad (\text{C11})$$

where  $\Delta_{\delta,\sigma'\sigma} = \chi_{\sigma'\sigma} \phi_\delta$  is used in the first line. Therefore, at the minimum of the grand potential, when  $\partial_{\chi_{\sigma'\sigma}} \Omega = 0$  we have

$$\chi_{\sigma'\sigma}^* = \langle \hat{\chi}_{\sigma\sigma'}^\dagger \rangle, \quad (\text{C12})$$

where  $\langle \hat{\chi}_{\sigma\sigma'}^\dagger \rangle = \langle \hat{\chi}_{\sigma'\sigma}^* \rangle$ . Therefore

$$\hat{\Delta}_{\delta,\sigma\sigma'}^\dagger = \langle \hat{\Delta}_{\delta,\sigma\sigma'}^\dagger \rangle. \quad (\text{C13})$$

This verifies the superconductivity self-consistency relation.

#### APPENDIX D: FURTHER NUMERICAL DETAILS: GRAND POTENTIAL, ORDER PARAMETERS, AND TEMPERATURE

In this Appendix we provide further numerical details in obtaining the phase diagrams in Figs. 3(a) and 4(a). Different choices of order parameters for magnetism and superconductivity are used to compute the grand potential in a self-consistent manner. The phase for a given filling is determined by the order parameter  $(\Delta_\alpha, m_\alpha)$  that yields the lowest  $\Omega$ . Figures 5(a) and 5(b) show  $\Omega$  and  $\Omega - \langle \Omega \rangle$ , respectively, for  $U_1/U_0 = -0.8$  at  $k_B T = 0$ . From them we can fix the phases as the filling per site of the system increases from 0 to 2. These phases are visualized in Figs. 3 and 4 (for the dependence on the temperature, see our discussion below).

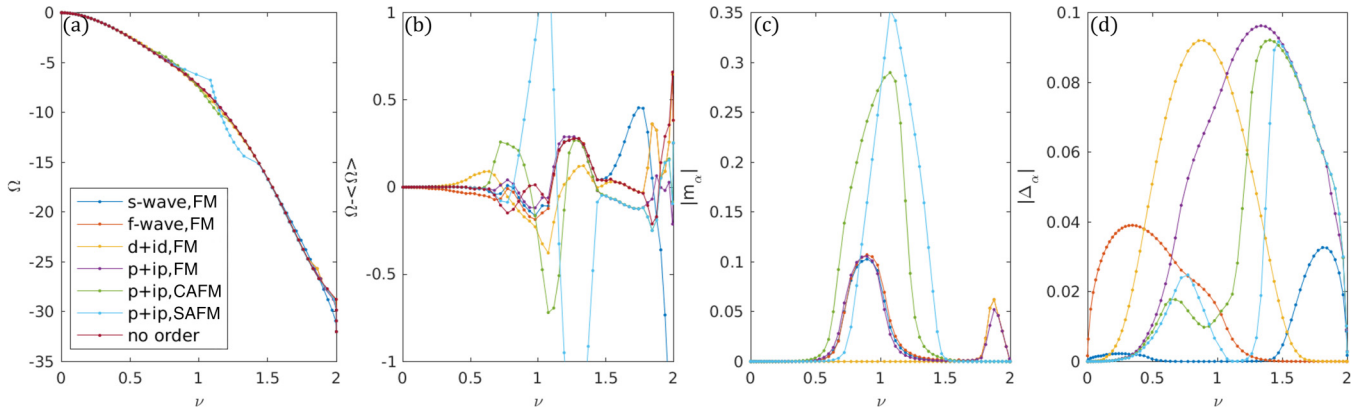


FIG. 5. (a) Grand potential  $\Omega$  at  $U_1/U_0 = -0.8$  is plotted for different choices of order parameters ( $\Delta_\alpha, m_\alpha$ ) indicated in the legend. (b)  $\Omega - \langle\Omega\rangle$  provides the magnified view of the grand potential for the same set of the order parameters ( $\Delta_\alpha, m_\alpha$ ). The legend in (a) is shared in the other panels. The order parameters with the lowest  $\Omega$  for a given  $\nu$  make the phase diagram that is shown in Fig. 3(a). (c) and (d) The magnitude of the magnetism (superconductivity) order parameters  $m_\alpha$  ( $\Delta_\alpha$ ) is plotted. The computation is performed at  $k_B T = 0$ .

Figures 5(c) and 5(d) show the order parameter of magnetism and that of superconductivity, respectively. The color indicates choices of order parameters, sharing the same legend as in Fig. 5(a). The appearance of a large order parameter for a given filling implies the existence of a preferred phase. For example, the order parameters of CAFM and SAFM are peaked, and in Fig. 5(c) we can spot that CAFM and SAFM with  $p + ip$  superconductivity have the lowest  $\Omega$  in  $\nu \in [1, 1.5]$  in turn. Figure 5(d) verifies that  $f$ -wave,  $(d + id)$ -wave, and  $(p + ip)$ -wave superconductivity order parameters take large values from low to high filling. Near  $\nu = 2$ , however, the  $s$ -wave superconductivity is dominantly preferred even though its order parameter is smaller than others. As shown in Fig. 4(b), not only the magnitude of the converged order parameter but also the position of the Fermi surface and the location of nodes of the order parameter play critical roles

in lowering the grand potential. Lastly, notice that the legend of Fig. 4(a) is different from that of Fig. 5(a). The latter always comes with one magnetic and one superconductivity order parameter, while the former has phases with only one of them, such as the “ $s$ -wave,” “ $d + id$ ,” “ $p + ip$ ,” and “FM” phases. This is because in Figs. 5(c) and 5(d) some order parameters converge to zero, thus showing no corresponding order. For example, the phase “ $s$ -wave, FM” near  $\nu = 2$  has no magnetic order. The phase “ $d + id$ , FM” has zero magnetism at  $\nu \simeq 0.9$ . The phases “ $p + ip$ , FM,” “ $p + ip$ , CAFM,” and “ $p + ip$ , SAFM” have zero magnetic order in  $\nu \in [1.5, 1.75]$ . Figure 6 shows the temperature dependence of the superconductivity (top row) and magnetism (bottom row) order parameters for  $U_1/U_0 = -0.8$ . We have six combinations of the two order parameters indicated in Fig. 5(a). Our formalism introduced in Sec. III is applicable to a finite temperature, and Fig. 6 directly

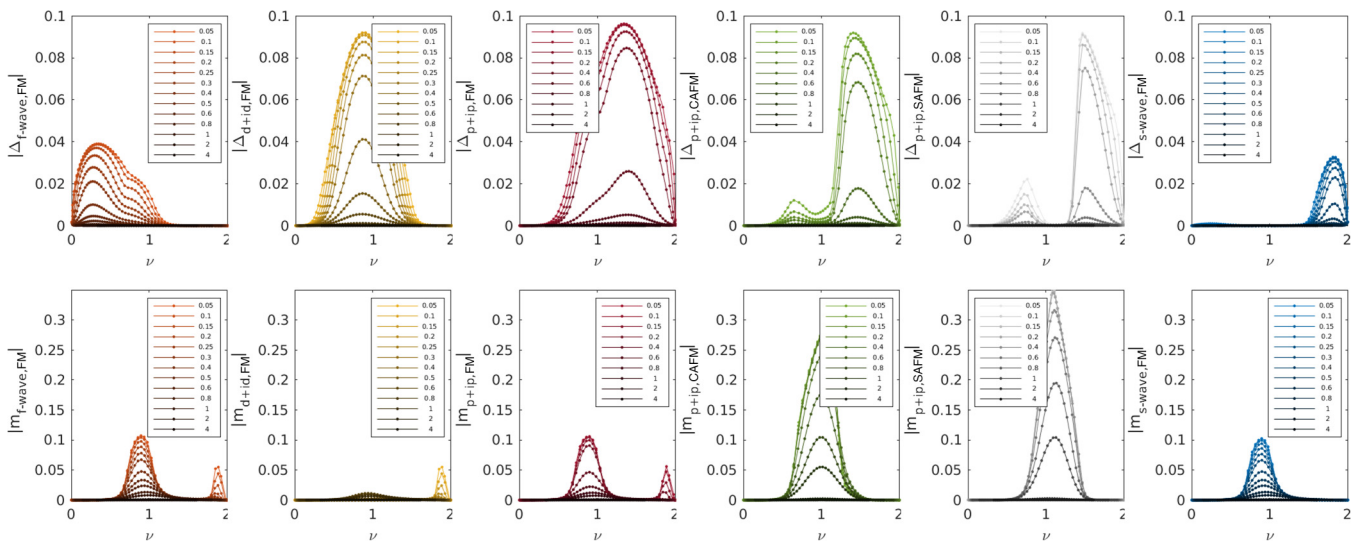


FIG. 6. The order parameters are shown for different temperatures,  $k_B T/|t_1| \in [0.05, 4]$ . The zero-temperature values are shown in Figs. 5(c) and 5(d). The top (bottom) row shows the superconductivity (magnetism) order parameters for the six different choices indicated in Fig. 5(a). The peaks of the superconductivity order parameters  $\Delta_\alpha$  do not overlap with the peaks of the magnetic parameters  $m_\alpha$  for singlet-pairing cases [ $s$ -wave and  $(d + id)$ -wave symmetries], while the coexistence of superconductivity and magnetism is shown for triplet-pairing cases [ $(p + ip)$ -wave and  $f$ -wave symmetries].

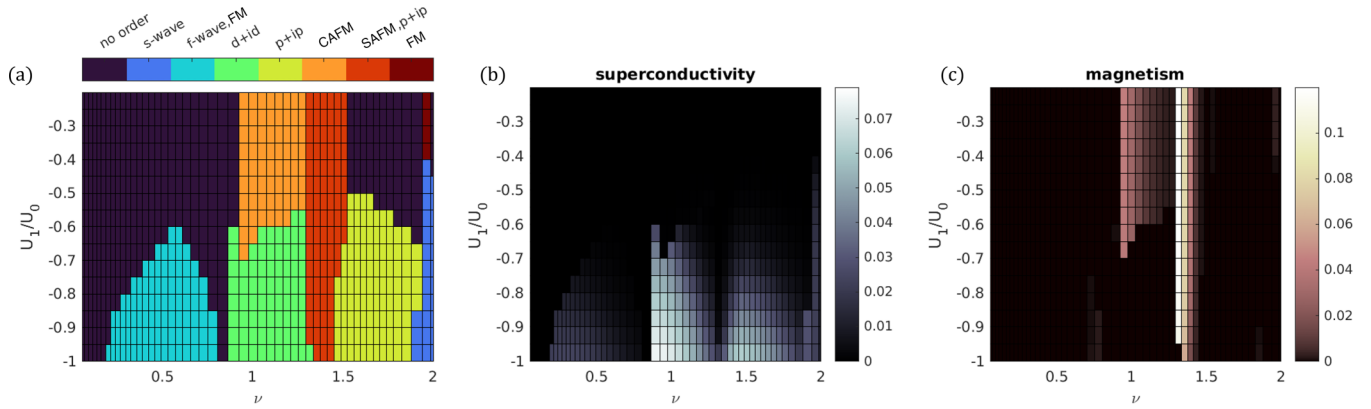


FIG. 7. (a) The phase diagram for  $U_0 = 4|t_1|$ . (b) and (c) The same set of superconducting and magnetism phases appear in the domain of attractive interaction  $U_1$  and filling  $\nu$ . Near the half filling  $\nu \simeq 1$ , the two types of antiferromagnetism (CAFM and SAFM) are positioned, and the superconducting order parameters increase with  $|U_1|$ . From low to high filling,  $f$ -wave,  $(d + id)$ -wave,  $(p + ip)$ -wave, and  $s$ -wave pairings are preferred in a similar manner to  $U_0 = 6|t_1|$  in Fig. 4. Due to its reduced on-site repulsive interaction, CAFM is preferred to ferromagnetism right below  $\nu = 1$ .

shows the suppression of the order parameters with increasing temperature. Note that singlet superconducting pairing [ $s$ -wave and  $(d + id)$ -wave symmetries] does not prefer the coexistence with magnetism (FM), while the triplet pairing [ $(p + ip)$ -wave and  $f$ -wave symmetries] shows a finite overlap with magnetism (ferromagnetism, CAFM, and SAFM). All the numerical results presented so far are for repulsive on-site interaction  $U_0 = 6|t_1|$ , which is about half of the bandwidth. Figure 7(a) shows the phase diagram at  $U_0 = 4|t_1|$ . It shares overall generic features with the phase diagram in Fig. 4, and the same set of magnetism and superconducting

phases appear with varying filling  $\nu$  and attractive interaction strength  $U_1$ . The two types of antiferromagnetism (CAFM and SAFM) appear in  $\nu \in [1, 1.5]$ , and the ferromagnetism appears near  $\nu = 2$ . Due to the reduced repulsive interaction, the ferromagnetism is not developed at half filling in this case. At  $|U_1/U_0| > 0.5$ , superconducting phases [ $f$ -wave,  $(d + id)$ -wave,  $(p + ip)$ -wave, and  $s$ -wave symmetries] take place. For  $f$ -wave and  $(p + ip)$ -wave triplet-spin-pairing superconducting phases, ferromagnetism and SAFM phases are found to coexist [see overlapping regimes of nonzero order parameters in Figs. 7(b) and 7(c)].

- 
- [1] F. Ming, S. Johnston, D. Mulugeta, T. S. Smith, P. Vilmercati, G. Lee, T. A. Maier, P. C. Snijders, and H. H. Weitering, Realization of a hole-doped Mott insulator on a triangular silicon lattice, *Phys. Rev. Lett.* **119**, 266802 (2017).
- [2] F. Ming, T. S. Smith, S. Johnston, P. C. Snijders, and H. H. Weitering, Zero-bias anomaly in nanoscale hole-doped Mott insulators on a triangular silicon surface, *Phys. Rev. B* **97**, 075403 (2018).
- [3] X. Wu, F. Ming, T. S. Smith, G. Liu, F. Ye, K. Wang, S. Johnston, and H. H. Weitering, Superconductivity in a hole-doped Mott-insulating triangular adatom layer on a silicon surface, *Phys. Rev. Lett.* **125**, 117001 (2020).
- [4] F. Ming, X. Wu, C. Chen, K. D. Wang, P. Mai, T. A. Maier, J. Strokoz, J. Venderbos, C. González, J. Ortega, S. Johnston, and H. H. Weitering, Evidence for chiral superconductivity on a silicon surface, *Nat. Phys.* **19**, 500 (2023).
- [5] S. Modesti, L. Petaccia, G. Ceballos, I. Vobornik, G. Panaccione, G. Rossi, L. Ottaviano, R. Larciprete, S. Lizzit, and A. Goldoni, Insulating ground state of Sn/Si(111)- $(\sqrt{3} \times \sqrt{3})R30^\circ$ , *Phys. Rev. Lett.* **98**, 126401 (2007).
- [6] G. Profeta and E. Tosatti, Triangular Mott-Hubbard insulator phases of Sn/Si(111) and Sn/Ge(111) surfaces, *Phys. Rev. Lett.* **98**, 086401 (2007).
- [7] G. Li, M. Laubach, A. Fleszar, and W. Hanke, Geometrical frustration and the competing phases of the Sn/Si(111)  $\sqrt{3} \times \sqrt{3}R30^\circ$  surface systems, *Phys. Rev. B* **83**, 041104(R) (2011).
- [8] G. Li, P. Höpfner, J. Schäfer, C. Blumenstein, S. Meyer, A. Bostwick, E. Rotenberg, R. Claessen, and W. Hanke, Magnetic order in a frustrated two-dimensional atom lattice at a semiconductor surface, *Nat. Commun.* **4**, 1620 (2013).
- [9] B. Davoudi, S. R. Hassan, and A. M. S. Tremblay, Competition between charge and spin order in the  $t$ - $U$ - $V$  extended Hubbard model on the triangular lattice, *Phys. Rev. B* **77**, 214408 (2008).
- [10] L. F. Tocchio, C. Gros, X.-F. Zhang, and S. Eggert, Phase diagram of the triangular extended Hubbard model, *Phys. Rev. Lett.* **113**, 246405 (2014).
- [11] J. Chen, F. Petocchi, and P. Werner, Causal versus local  $GW + \text{EDMFT}$  scheme and application to the triangular-lattice extended Hubbard model, *Phys. Rev. B* **105**, 085102 (2022).
- [12] J. Willsher, H.-K. Jin, and J. Knolle, Magnetic excitations, phase diagram, and order-by-disorder in the extended triangular-lattice Hubbard model, *Phys. Rev. B* **107**, 064425 (2023).
- [13] M. Cheng, K. Sun, V. Galitski, and S. Das Sarma, Stable topological superconductivity in a family of two-dimensional fermion models, *Phys. Rev. B* **81**, 024504 (2010).
- [14] S. Wolf, T. L. Schmidt, and S. Rachel, Unconventional superconductivity in the extended Hubbard model: Weak-coupling renormalization group, *Phys. Rev. B* **98**, 174515 (2018).
- [15] Y.-F. Jiang and H.-C. Jiang, Topological superconductivity in the doped chiral spin liquid on the triangular lattice, *Phys. Rev. Lett.* **125**, 157002 (2020).

- [16] S. Wolf, D. Di Sante, T. Schwemmer, R. Thomale, and S. Rachel, Triplet superconductivity from nonlocal Coulomb repulsion in an atomic Sn layer deposited onto a Si(111) substrate, *Phys. Rev. Lett.* **128**, 167002 (2022).
- [17] M. Biderang, M.-H. Zare, and J. Sirker, Topological superconductivity in Sn/Si(111) driven by nonlocal Coulomb interactions, *Phys. Rev. B* **106**, 054514 (2022).
- [18] S. Onari, R. Arita, K. Kuroki, and H. Aoki, Phase diagram of the two-dimensional extended Hubbard model: Phase transitions between different pairing symmetries when charge and spin fluctuations coexist, *Phys. Rev. B* **70**, 094523 (2004).
- [19] D. L. Bergman and T. Pereg-Barnea, The origin of Tc enhancement in heterostructure cuprate superconductors, *Materials* **4**, 1835 (2011).
- [20] D. Scalapino, The case for  $d_{x^2-y^2}$  pairing in the cuprate superconductors, *Phys. Rep.* **250**, 329 (1995).
- [21] The explicit expression of  $\epsilon_{\vec{k}}$  is as follows:

$$\epsilon_{\vec{k}} = -2t_1 \left[ \cos(k_x) + 2 \cos\left(\frac{\sqrt{3}}{2}k_y\right) \cos\left(\frac{k_x}{2}\right) \right] - 2t_2 \left[ \cos(\sqrt{3}k_y) + 2 \cos\left(\frac{3}{2}k_x\right) \cos\left(\frac{\sqrt{3}}{2}k_y\right) \right]$$

$$\begin{aligned} & -2t_3[\cos(2k_x) + 2 \cos(k_x) \cos(\sqrt{3}k_y)] \\ & -4t_4 \left[ \cos\left(\frac{5}{2}k_x\right) \cos\left(\frac{\sqrt{3}}{2}k_y\right) + \cos(2k_x) \cos(\sqrt{3}k_y) \right. \\ & \left. + \cos\left(\frac{k_x}{2}\right) \cos\left(\frac{3\sqrt{3}}{2}k_y\right) \right] \\ & -2t_6[\cos(2\sqrt{3}k_y) + 2 \cos(3k_x) \cos(\sqrt{3}k_y)], \end{aligned}$$

where the fifth-nearest-neighbor hopping strength  $t_5 = 0$ .

- [22] For a finite size of grid in momentum space, energy eigenvalues take discrete values. Thus, when the chemical potential is tuned continuously, the filling discontinuously changes, and in turn so does the total energy. This discontinuity is not favored for the comparison of the total energies of phases with different order parameters for a given filling. To remove this issue, we choose the temperature  $k_B T/|t_1| = 0.1$ , which is about three times larger than the mean level spacing.
- [23] TUDelft OpenCourseWare, <https://ocw.tudelft.nl/course-readings/particle-hole-symmetry/>.